ed from whole blood by Puregene (Gentra System). The sense primer 5′-CAGRGCCGCGGCTTTCT-TCTC-3′ and the antisense primer 5′-CTACAACG-GCAGAAGAGGAC-3′ were designed to amplify the 172-bp NH_2-terminal region of HOXD13 containing the 15 alanine residues. PCR was performed with [α-^{32}P]deoxycytidine 5′-triphosphate (dCTP) (10 mM, 3000 Ci/mmol) added to the reaction. The condition was 35 cycles at 94°C for 0.5 min, 60°C for 1 min, 72°C for 2 min, with initial heating at 95°C for 2 min and, after all 35 cycles were completed, additional heating at 72°C for 10 min. PCR reactions were performed in a total volume of 10 μl containing 1× PCR buffer, 0.75 mM $MgCl_2$, 200 μM deoxynucleotide triphosphate (dNTP) without dGTP, 200 μM 7-deaza-2′-deoxyguanosine 5′-triphosphate, a final concentration of 0.5 μM for each primer, 10% dimethyl sulfoxide, and 0.2 U of Taq polymerase. The PCR products were analyzed on a 5% polyacrylamide gel under nondenaturing conditions. PCR products from affected individuals were subcloned into pCRII (Invitrogen) and subjected to cycle sequencing.

18. S. Hayashi and M. P. Scott, *Cell* **63**, 883 (1990).
19. J. B. Jaynes and P. H. O'Farrell, *Nature* **336**, 744 (1988).
20. J. D. Licht, M. J. Grossel, J. Figge, U. M. Hansen, *ibid.* **346**, 76 (1990).
21. K. Han and J. L. Manley, *Genes Dev.* **7**, 491 (1993).
22. ———, *EMBO J.* **12**, 2723 (1993).
23. P. Dolle *et al.*, *Cell* **75**, 431 (1993).
24. Y. Yokouchi, H. Sasaki, A. Kuroiwa, *Nature* **353**, 443 (1991).
25. P. Dolle, J. C. Izpisua-Belmonte, E. Boncinelli, D. Duboule, *Mech. Dev.* **36**, 3 (1991).
26. N. H. Shubin and P. Alberch, *Evol. Biol.* **20**, 319 (1986).
27. P. Sordino, F. van der Hoeven, D. Duboule, *Nature* **375**, 678 (1995).
28. B. Rogina and W. B. Upholt, *Nucleic Acids Res.* **21**, 1316 (1993).
29. The cosmid clone G2, containing the *HOXD13* gene, was provided by E. Boncinelli. We want to thank C. Tabin for helpful discussions. Y. Pittel provided secretarial assistance. Supported by NIH grants AR36819 and AR36820 (to B.R.O.) and Deutsche Forschungsgemeinschaft (to S.M.).

18 January 1996; accepted 13 March 1996

Interactions Between Electrical Activity and Cortical Microcirculation Revealed by Imaging Spectroscopy: Implications for Functional Brain Mapping

Dov Malonek and Amiram Grinvald

Modern neuroimaging techniques use signals originating from microcirculation to map brain function. In this study, activity-dependent changes in oxyhemoglobin, deoxyhemoglobin, and light scattering were characterized by an imaging spectroscopy approach that offers high spatial, temporal, and spectral resolution. Sensory stimulation of cortical columns initiates tissue hypoxia and vascular responses that occur within the first 3 seconds and are highly localized to individual cortical columns. However, the later phase of the vascular response is less localized, spreading over distances of 3 to 5 millimeters.

Regional changes in cerebral blood flow and blood oxygenation "co-localize" with regions of increased neuronal activity (*1*, *2*). Signals that reflect these changes have been used by positron-emission tomography (PET) and functional magnetic resonance imaging (f-MRI) to both understand cortical metabolism and investigate cognitive and perceptual processes by rapid identification of functionally distinct cortical areas (*3*, *4*). Furthermore, the study of spatial relationships between individual cortical columns within a given brain area has become feasible with optical imaging based on intrinsic signals, at a spatial resolution of about 50 μm (*5*–*7*). However, there are outstanding controversies concerning whether cortical metabolism is aerobic or anaerobic, and indeed, the physiological events underlying these secondary signals have not been fully assessed (*2*, *3*). It is necessary to clarify the spatiotemporal characteristics of the intrinsic signals (*8*) in order to reveal the electrical activity underlying these signals and assess cognitive functions. Such clarification would set fundamental limits on the spatial and temporal resolutions for several functional brain imaging techniques.

Here we characterize the spatial precision and dynamics of blood oxygenation signals using in vivo intrinsic optical signals reflected from the exposed visual cortex. Previous optical imaging studies (*5*, *9*) suggested that the intrinsic signal observed in vivo is composed of several components, each of which reflects different vascular and metabolic sources. However, the temporal dynamics and spatial precision of these components were not determined.

To identify the spatiotemporal characteristics of the individual components of the intrinsic signal at many cortical locations, we designed the imaging spectroscope illustrated schematically in Fig. 1. A narrow, slitlike region from the exposed cortex of an anesthetized cat was projected onto a dispersing grating and focused on the camera detector. The image thus obtained represents multiple displaced versions of the isolated "slitlike cortical image," each of which is displaced as a function of wavelength. From the intensity variations in this spatiospectral image (y'', λ), we obtained the reflection spectrum of each imaged cortical point. In other words, the intensity profile of each horizontal line represented the reflection spectrum of a given location in the imaged cortex. The intensity profile along a vertical line represented the spatial pattern of cortical activation at a given wavelength. During the experiment, a sequence of such spatiospectral images was recorded after sensory stimulation.

Several important features of the spatiospectral image are immediately apparent in Fig. 2. Large absorption (lower intensity of reflection, dark image) is evident at the wavelength range of 500 to 600 nm, and significantly less light was absorbed (higher intensi-

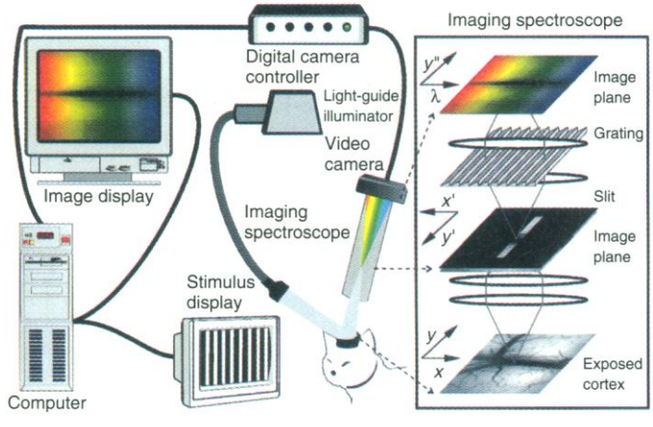

Fig. 1. The system for standard optical imaging (*6*, *11*, *22*). The inset at the right shows the scheme of the imaging spectroscope. It contains two tandem-lens macroscopes, diffraction grating (*22*), and an opaque disk with a transparent slit. The cortical surface (bottom image) is illuminated with white light (λ = 500 to 700 nm) and imaged through the first macroscope onto the first image plane, where an opaque disk with a slit is positioned. The light thus isolated is collimated, passed through a diffraction grating whose light dispersion is perpendicular to the slit, and then focused on the camera target (top image). The axes show the different optical transformations that the cortical image undergoes. Temporal resolution was up to 100 ms. Spectral resolution, 1 to 4 nm.

Department of Neurobiology, Weizmann Institute of Science, Rehovot 76100, Israel.

ty of reflection, light image) at the 660 nm end of the spectral image (Fig. 2B). The fuzzy dark regions in the spatiospectral maps originate primarily from the decreased reflection resulting from increased absorption by capillaries, small arterioles, and venules at a wavelength range of 500 to 600 nm. These multiple spectra (intensity variations along horizontal lines) were in good agreement with hemoglobin reflection spectra measured from scattering tissue (*10*).

We started by mapping orientation columns in cat area 18 using standard optical imaging (*7*, *11*). Functional maps for orientation were obtained by computing the difference between cortical images obtained during stimulation by full-field, moving gratings of orthogonal orientations. Next, we selected the position for the "slitlike cortical image" (Fig. 2A) so that it contained several clearly segregated iso-orientation domains (~0.5 mm across) (arrows in Fig. 2C) and repeated the experiment after positioning the slit and diffraction grating in the imaging spectroscope (Fig. 1). Spatiospectral activity maps were computed in a fashion similar to that of standard maps (*6*, *7*). First, the difference between responses to an effective stimulus, such as the moving gratings, and a control blank stimulus was obtained. Throughout this report, we will refer to such a map as the global map and to the underlying signals as global signals. Second, the differences between responses to gratings of orthogonal orientations were evaluated. We will refer to these maps as differential orientation maps and to the corresponding signals as mapping signals. The resulting spatiospectral maps contain the global and mapping signals acquired simultaneously not only at multiple cortical locations but also at multiple wavelengths.

A differential orientation map in the spatiospectral domain is shown in Fig. 2D. The pattern of intensity variation along the vertical axis (spatial domain) was similar at all wavelengths, although its amplitude was not constant, appearing as long, horizontal dark and light bands. Thus, cortical locations marked by the dark bands were preferentially activated by the vertical grating, whereas those marked by light bands, by the horizontal grating (*5*, *6*). From the classical studies of Hubel and Wiesel (*12*), it is well known that vertical gratings produce spiking activity in areas that would correspond to regions marked here by the dark bands, whereas horizontal gratings electrically activate only regions marked here by the light bands (*7*).

A sequence of global maps in the spatiospectral domain is shown in Fig. 2E. No visible indications for different functional domains were seen in these global maps. This lack of functional segregation is surprising given the single unit mapping results discussed in the previous paragraph (*12*). This lack of segregation indicates that the activity-dependent global signals were not confined to regions of increased spiking activity; some components of the global signals exist beyond the cortical sites of spiking activity. To extract the average reflection spectra from each global map (Fig. 2E), we averaged the rows from all cortical regions that did not contain large blood vessels (Fig. 2G). Pronounced changes of the spectrum shape as a function of time were detected. These spectra are most informative, acting like fingerprints; for example, the shape of frame 3 reflects primarily the activity-dependent increase in deoxyhemoglobin, whereas the shape of frame 9 reflects primarily oxyhemoglobin increase and deoxyhemoglobin decrease (Fig. 2G, inset; compare to Fig. 2H, inset).

The time course of the differential orientation maps (mapping signals) in the spatiospectral domain is shown in Fig. 2F. In contrast with the images of the global signals, here we observed interlaced dark and light horizontal bands. Thus, functional domains that were selective for vertical or horizontal stimuli were clearly apparent at all imaged wavelengths. The averaged spectra of the mapping signals are shown in Fig. 2H (*13*). The temporal behavior of the mapping spectra is markedly different from the global spectra: they decayed to baseline much more slowly than the global signals. Again, these spectra serve as fingerprints: The shape of the first three spectra reflects primarily a difference in deoxyhemoglobin, and in later frames, the contribution of oxyhemoglobin is observed but is much less pronounced than that observed in the global spectra.

To test whether the activity-dependent changes in the average reflection spectra observed here could be accounted for primarily

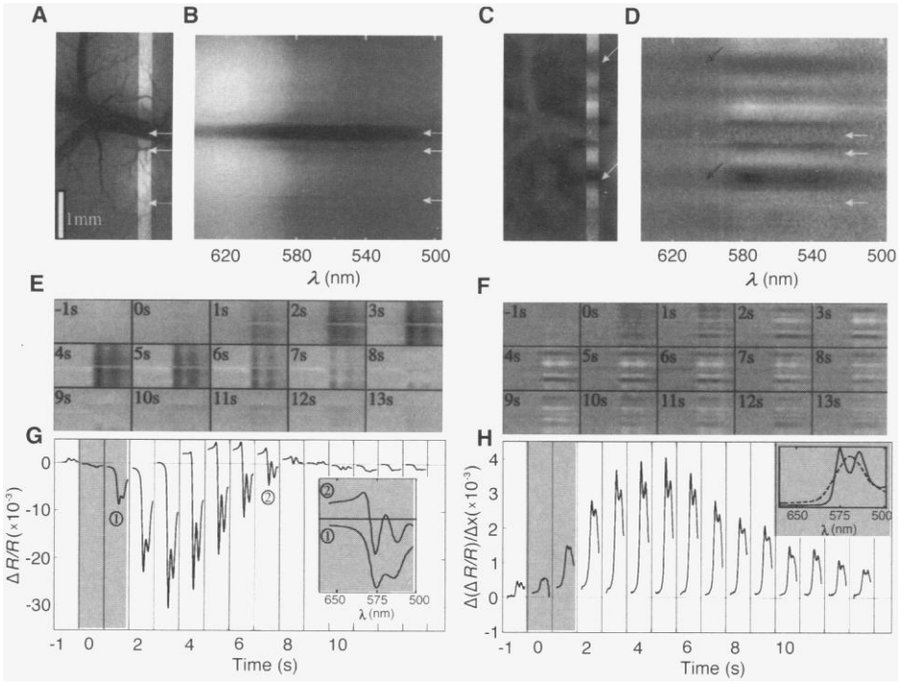

Fig. 2. Principles of optical imaging spectroscopy. (**A**) Cortical surface, illuminated at 570 nm. The slitlike cortical image is highlighted. (**B**) Spatiospectral image obtained while the cortex was illuminated with broad spectrum light. An increase in light absorption is seen at wavelengths below 600 nm (darkening). The fuzzy dark regions show signals from the capillary bed. The sharp, horizontal dark lines show the absorption spectra of superficial blood vessels (white arrows in A, B, and D). (**C**) Orientation map calculated for the slitlike cortical region (λ = 605 nm). (**D**) Spatiospectral orientation map. In both (C) and (D), the wide dark bands show cortical regions selective for vertical stimuli (oblique arrows). Dark and light thin lines correspond to signals from superficial blood vessels. (**E**) Time course of the global signal after 2 s of stimulation (wavelength range, 520 to 650 nm). Each frame is a spatiospectral image that shows reflection spectra (horizontal axis) obtained from 6 mm of cortical surface (vertical axis). This series was obtained by subtracting images acquired during blank stimulus presentation from images acquired during gratings presentation. The most pronounced features of these maps were the dark vertical stripes that peaked at 540 and 580 nm, corresponding to oxyhemoglobin absorption, which appeared at all cortical locations. The locations of horizontal thin lines coincide with the locations of superficial blood vessels. (**F**) Time course of the mapping signal after the 2 s of stimulation, obtained by subtracting responses to vertical stimuli from responses to horizontal stimuli. (**G**) Time course of the average global spectra. (Inset) Two expanded spectra obtained from frames 3 and 9. (**H**) Time course of the average mapping spectra (*13*). (Inset) Textbook absorption spectra of oxy (solid line) and deoxy (dotted line) hemoglobin. The double peak (increase in HbO_2) appears clearly only after about 2 s.

by activity-dependent hemodynamics and light scattering changes, the individual spectra changes (Fig. 2G) were fitted (*14*) to the textbook spectra of oxyhemoglobin, deoxyhemoglobin, and light scattering components (HbO_2, Hbr, and LS, respectively) (Fig. 3A). A good fit between the model and the experimental results was obtained. The amplitudes of all three components (HbO_2 and the late phases of Hbr and LS) increased with increased stimulus duration from 0.5 to 8 s. However, further increasing stimulus duration beyond 8 s produced no further increase in amplitude or time to peak. The signals remained elevated for as long as the stimulus persisted and returned to baseline some 4 to 6 s after the stimulus was terminated. These changes in Hbr and HbO_2 tissue concentrations were presumably caused by the net effect of changes in oxygen extraction, cerebral blood flow, and blood volume.

The mapping components but not the global components co-localized with the columnar architecture. Therefore, we extracted the individual mapping components by computing the difference between two time series of spatiospectral images, each of which was obtained after grating stimulus of orthogonal orientations (*15*). The time course in Fig. 3B illustrates the activity-dependent spatial pattern of each component (mapping signal). Intensity changes along a horizontal line represent the time course at a given cortical location. Intensity changes along a vertical line represent the amplitude of the mapping signal at different cortical locations at a given time. The orientation bands are apparent for the Hbr and LS components but are much fuzzier for the HbO_2 component.

To quantify the spatial precision of the various components, we computed the ratio between the amplitudes of the global signals and mapping signals for each component. This ratio offers a quantitative measure of the relative spatial precision of each component. We defined the instantaneous amplitude of each mapping component as the average amplitude in space at a given time. A marked difference in the average time course of each mapping component was observed (Fig. 3C). The Hbr component linearly increased throughout stimulus, a duration of 1 to 6 s, and decayed for more than 15 s. The latency to the onset and the peak of the HbO_2 was larger than that of the Hbr by 1 to 2 s. The LS component is faster in latency, rise time, and decay time relative to the Hbr component. At 2 s, the magnitude of the Hbr mapping component comprised 31 ± 6% (SD, $N = 4$) of its global component. For the HbO_2 it was only 4.5 ± 1.5% at its maximum. For the LS component, the ratio was 21 ± 7% at 2 s (*16*). These ratios suggested that the early Hbr mapping components were 6- to 10-fold more localized than the HbO_2 mapping component.

Our results shed light on several controversies raised by previous PET and f-MRI studies. We confirmed that sensory stimulation gives rise to a large increase in blood oxygenation. However, neither PET nor most f-MRI studies observed an initial increase in deoxyhemoglobin ("initial dip"), and hence, both postulated an initial phase of anaerobic metabolism. Our observations (*17*) revealed an early increase in deoxyhemoglobin concentration (Fig. 2G, inset, and Fig. 3A, middle panel), consistent with direct Po_2 measurements from other groups (*18*) and indicating that aerobic metabolism took place immediately after sensory stimulation. Recently, two f-MRI studies confirmed the results derived from optical imaging (*19*). Because the optical signals shown here originated primarily from the capillaries, the failure of most f-MRI studies to detect the initial dip and visualize cortical columnar organization raises the possibility that these measurements were not sufficiently sensitive to signals from the capillaries. It remains to be seen whether the spatial resolution of f-MRI can be improved by stimulation protocols and data analysis procedures similar to those used during optical imaging.

The above spectroscopic data suggest the following sequence of three different physiological events after a brief sensory stimulation. First, the initial increase in deoxyhemoglobin (Fig. 3A) indicated that a localized increase of neuronal activity was accompanied by aerobic metabolism. This metabolic process develops local gradients of tissue oxygen levels (Fig. 3, B and C) between active and inactive regions (spiking). Surprisingly, even though we clearly detected the increase in deoxyhemoglobin, the complementary reduction in oxyhemoglobin was very small if it existed at all (Fig. 3, A and B). This observation suggests that a second physiological event immediately compensated for the initial oxyhemoglobin decrease. Previous reports (*20*) have suggested that a fast and highly localized blood volume and flow redistribution in the capillaries may account for this cancellation. The third event was the delayed increase of the global oxyhemoglobin and the delayed undershoot of the global deoxyhemoglobin signals presumably caused by the well-known, large activity-dependent increase of blood volume and flow to the tissue. Furthermore, this late blood-flow and volume change must be regulated at rather a coarse spatial scale because they do not quickly eliminate the local gradients in deoxyhemoglobin (mapping signal) created by increased electrical activity, which instead con-

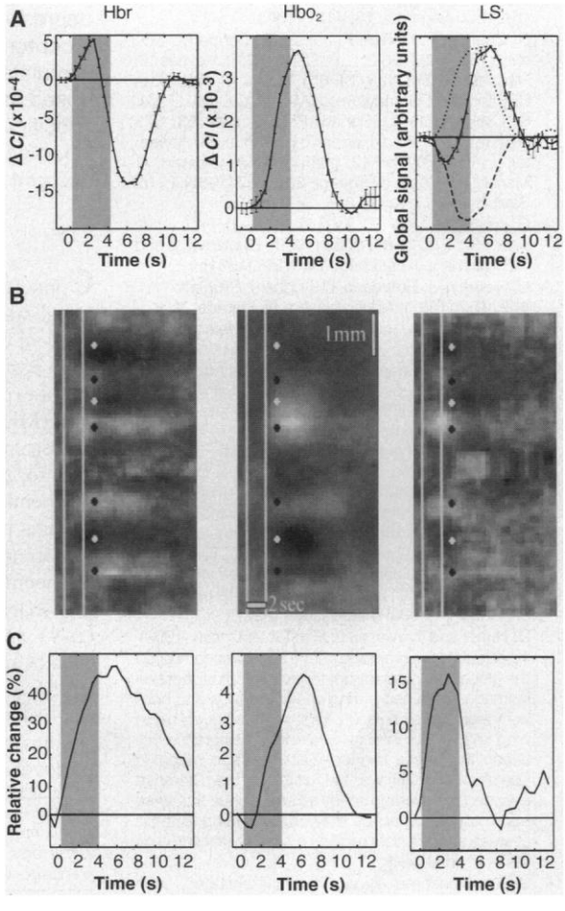

Fig. 3. (**A**) Time courses of the global signals for the Hbr, HbO_2, and LS components. Error bars (±1 SD, $N = 4$) were calculated for four repeated measurements from the same cortical region (4-s stimuli). The decrease in deoxyhemoglobin started before stimulus termination. The time and amplitude of this peak was insensitive to stimulus duration above 2 s. ΔC is a change in tissue concentration and l is the path length of light in the tissue. Both Hbr and HbO_2 are measured in the same arbitrary units. Two models were used to examine the LS contribution (*14*): (i) one wavelength-independent component (solid line), and (ii) a wavelength-independent component (dotted line) plus a λ^{-4} component (dashed line). The three LS curves (*16*) were normalized and plotted in arbitrary units. (**B**) Time course and spatial precision of maps produced by the Hbr, HbO_2, and LS components. Global components obtained while stimulating with vertical gratings were compared to those obtained while stimulating with horizontal gratings; their difference is illustrated here. Black and white crosses mark the orientation columns in same cortical loci and the same time in all three panels. The wavelength range of 520 to 650 nm was integrated. Each map was scaled independently. (**C**) Average time course of the mapping signals.

tinued to decay very slowly (compare middle panels of Fig. 3, A and C). This large mismatch between oxygen consumption and supply probably underscores the importance of adequate oxygen supply: watering the entire garden for the sake of one thirsty flower (*21*).

REFERENCES AND NOTES

1. C. Roy and C. Sherrington, *J. Physiol.* **11**, 85 (1890); J. Olesen, *Brain* **94**, 635 (1971); J. Risberg and D. Ingvar, *Brain Res.* **96**, 737 (1973); M. Kato, H. Ueno, P. Black, *Exp. Neurol.* **42**, 65 (1974); J. Greenberg, P. Hand, A. Sylvestro, M. Reivich, *Acta Neurol. Scand.* **60**, 12 (1979); C. Iadecola, *Trends Neurosci.* **16**, 206 (1993)
2. P. Fox and M. Raichle, *Ann. Neurol.* **17**, 303 (1985); L. Sokoloff *et al.*, *J. Neurochem.* **28**, 897 (1994); N. A. Lassen and D. H. Ingvar, *Experientia* **17**, 42 (1961).
3. M. Raichle, *Sci. Am.* **270**, 58 (April 1994); P. T. Fox *et al.*, *Nature* **323**, 806 (1986); P. Fox and M. Raichle, *Proc. Natl. Acad. Sci. U.S.A.* **83**, 1140 (1986); P. T. Fox, M. E. Raichle, M. A. Mintun, C. Dence, *Science* **241**, 462 (1988).
4. S. Ogawa, T. Lee, A. Kay, *Proc. Natl. Acad. Sci. U.S.A.* **87**, 9868 (1990); J. W. Belliveau *et al.*, *Science* **254**, 716 (1991); K. Kwong *et al.*, *Proc. Natl. Acad. Sci. U.S.A.* **89**, 5675 (1992); S. Ogawa *et al.*, *ibid.*, p. 5951; R. Turner *et al.*, *Magn. Reson. Med.* **29**, 277 (1993).
5. A. Grinvald, E. Lieke, R. Frostig, C. Gilbert, T. Wiesel, *Nature* **324**, 361 (1986).
6. D. Y. Ts'o, R. D. Frostig, E. E. Lieke, A. Grinvald, *Science* **249**, 417 (1990); G. Blasdel, *J. Neurosci.* **12**, 3139 (1992); M. Weliky, K. Kandler, D. Fitzpatrick, L. C. Katz, *Neuron* **15**, 541 (1995); I. Godecke and T. Bonhoeffer, *Nature* **379**, 251 (1996).
7. T. Bonhoeffer and A. Grinvald, *Nature* **353**, 429 (1991); *J. Neurosci.* **13**, 4157 (1993).
8. B. Chance, P. Cohen, F. Jobsis, B. Schoener, *Science* **137**, 499 (1962); L. B. Cohen, R. D. Keynes, B. Hille, *Nature* **218**, 438 (1968); I. Tasaki, A. Watanabe, R. Sandlin, L. Carnay, *Proc. Natl. Acad. Sci. U.S.A.* **61**, 883 (1968); L. Cohen, *Physiol. Rev.* **53**, 373 (1973); F. Jobsis, J. Keizer, J. LaManna, M. Rosental, *J. Appl. Physiol.* **43**, 858 (1977); A. Grinvald, A. Manker, M. Segal, *J. Physiol.* **333**, 269 (1982); B. M. Salzberg *et al.*, *Nature* **306**, 36 (1983).
9. R. Frostig, E. Lieke, D. Ts'o, A. Grinvald, *Proc. Natl. Acad. Sci. U.S.A.* **87**, 6082 (1990); B. MacVicar and D. Hochman, *J. Neurosci.* **11**, 1458 (1991).
10. U. Heinrich, J. Hoffmann, D. Lubbers, *Pflugers Arch.* **409**, 152 (1987); M. Watanabe, N. Harada, H. Kosaka, T. Shiga, *J. Cereb. Blood Flow Metab.* **14**, 75 (1994).
11. Five cats were anesthetized with continuous infusion of sodium pentothal after an initial induction using ketamine HCl and atropine sulphate. All surgical and experimental procedures were in accordance with NIH guidelines. A craniotomy was performed, overlying area 18 of the visual cortex. A stainless steel chamber was mounted over the craniotomy. Each stimulus was presented 24 to 128 times, in randomized order. The intrinsic optical signals were imaged by a slow-scan CCD (charge-coupled device) camera (*6*) or enhanced video system (Imager 2001; Optical Imaging, Germantown) attached to a dual macroscope (*22*).
12. D. Hubel and T. Wiesel, *J. Physiol.* **160**, 106 (1962).
13. To calculate the mapping spectra, we first computed the global signal spectrum for every cortical location in images obtained during vertical-grating and horizontal-grating stimulation. Each spatiospectral mapping image was then calculated as a difference between the above images. Each average mapping spectrum (Fig. 2H) was calculated as the difference between the average spectra from regions that were maximally activated by the vertical grating and the average spectra from regions maximally activated by the horizontal grating.
14. Spectral decomposition: For small changes, each experimental spectrum can be expressed as

$$\Delta OD_\lambda = K_1\varepsilon(HbO_2) + K_2\varepsilon(Hbr) + LS$$

where K_1 is related to the product of increased HbO_2 tissue concentration and the optical path length; similarly, K_2 is the corresponding parameter for Hbr. The textbook extinction coefficients $\varepsilon(HbO_2)$ and $\varepsilon(Hbr)$ were used. A least squares routine was used to fit the experimental data (root mean square of error was <5%). LS was assumed constant. Using other wavelength-dependent models for the LS contribution did not significantly affect the values of K_1 and K_2. Modeling the contribution from cytochromes proved that at the wavelength range we used, their contribution to the observed spectral changes was minimal.
15. Each mapping component was calculated as a difference between the corresponding global components obtained during vertical and horizontal grating stimulation. We then calculated the difference in the average intensity in regions that were maximally selective for either stimulus.
16. A distinction between the various components of light scattering has not been made here. The LS signal is useful for functional optical imaging, whenever large vascular noise is associated with an experiment. High-quality functional maps were obtained at a wavelength longer than 660 nm, at which the contribution of light scattering to the mapping components was larger than 70%.
17. Both f-MRI and PET studies were performed on awake human subjects, whereas the present experiments were performed on anesthetized cats. However, we observed a similar "initial dip" in experiments performed on awake monkeys.
18. I. Silver, in *Cerebral Vascular Smooth Muscle and its Control*, K. Elliott and M. O'Connor, Eds. (Elsevier, New York, 1978), pp. 49–61.
19. R. Menon, X. Hu, P. Andersen, K. Ugurbil, S. Ogawa, *Proc. Soc. Magn. Reson.* **1**, 68 (1994); J. Henning, T. Ernst, O. Speck, G. Deuschl, E. Feifel, *Magn. Reson. Med.* **31**, 85 (1994).
20. W. Kuschinsky and O. Paulson, *Cerebrovasc. Brain Metab. Rev.* **4**, 261 (1992); U. Dirnagl (personal communication) visualized it directly using confocal microscopy.
21. R. Turner and A. Grinvald, *Proc. Soc. Magn. Reson.* **1**, 430 (1994).
22. H. Ratzlaff and A. Grinvald, *J. Neurosci. Methods* **36**, 127 (1991).

23. We thank U. Dirnagl, A. Villringer, I. Steinberg, A. Artsen, and R. Malach for their useful comments. We also thank I. Silver, P. Jezzard, B. Chance, and R. Turner for their helpful contribution. Special thanks to A. Ariel, D. Glaser, D. Shoham, A. Shmuel, and I. Vanzetta for their help during experiments and to N. Dekel, D. Ettner, C. Wijnbergen, and S. Leytus for their technical help.

7 December 1995; accepted 23 February 1996

Ocular Dominance Plasticity Under Metabotropic Glutamate Receptor Blockade

Takao K. Hensch and Michael P. Stryker*

Occluding vision through one eye during a critical period in early life nearly abolishes responses to that eye in visual cortex. This phenomenon is mimicked by long-term depression of synaptic transmission in vitro, which may require metabotropic glutamate receptors (mGluRs) and is age-dependent. Peaks in mGluR expression and glutamate-stimulated phosphoinositide turnover during visual cortical development have been proposed as biochemical bases for the critical period. Pharmacological blockade of mGluRs specifically prevented synapse weakening in mouse visual cortical slices but did not alter kitten ocular dominance plasticity in vivo. Thus, a heightened mGluR response does not account for the critical period in development.

Connections in the developing vertebrate visual system are sculpted by an activity-dependent competition between inputs for common postsynaptic neurons. Manipulations of visual experience, such as monocular deprivation (MD) during a well-defined critical period, regulate cortical physiology and ultimately lead to anatomical rearrangements (*1*). The biochemical basis for experience-dependent changes in visual circuitry remains largely unknown. mGluRs are reported to play a role in the neural plasticity of several systems, including synapse strengthening in the hippocampus (*2–4*) and long-term depression (LTD), a form of age-dependent (*5*) synapse weakening in the hippocampus (*6*), neocortex (*7*), and cerebellum (*8*). Expression of mGluRs (*9*) and glutamate-stimulated phosphoinositide (PI) turnover (*10*) have both been shown to peak transiently during development of cat primary visual cortex, concurrent with the height of sensitivity to visual deprivation. Thus, mGluR function is a candidate mediator of cortical plasticity, accounting for both the time course of the critical period and the loss of responsiveness from an eye deprived of vision. We have now examined developmental plasticity of primary visual cortex both in vitro and in vivo with the mGluR antagonist α-methyl-4-carboxyphenylglycine (MCPG).

The mechanisms responsible for the formation of ocular dominance columns during normal development are thought to underlie the effects of MD (*1*). At the peak of the critical period in the cat (4 weeks after birth), significant segregation of the afferent axons serving the two eyes has already taken place (*11*). Thus, we examined depotentiation of experimentally potentiated responses, rather than depression of naïve synapses, as the most appropriate in vitro model for the loss of responses through the deprived eye. Theta-burst stimulation (TBS), to produce

Neuroscience Graduate Program, W. M. Keck Foundation Center for Integrative Neuroscience, Department of Physiology, University of California, San Francisco, San Francisco, CA 94143–0444, USA.

*To whom correspondence should be addressed.